Construction of a Coronary Artery Atlas from CT Angiography

Pau Medrano-Gracia[1,*], John Ormiston[2], Mark Webster[3], Susann Beier[1], Chris Ellis[2], Chunliang Wang[4], Alistair A. Young[1], and Brett R. Cowan[1]

[1] Dept. Anatomy with Radiology, University of Auckland, New Zealand
p.medrano@auckland.ac.nz
[2] Auckland Heart Group, Auckland, New Zealand
[3] Auckland City Hospital, Auckland, New Zealand
[4] Center for Medical Image Science and Vis., Linköping University Hospital, Sweden

Abstract. Describing the detailed statistical anatomy of the coronary artery tree is important for determining the ætiology of heart disease. A number of studies have investigated geometrical features and have found that these correlate with clinical outcomes, e.g. bifurcation angle with major adverse cardiac events. These methodologies were mainly two-dimensional, manual and prone to inter-observer variability, and the data commonly relates to cases already with pathology. We propose a hybrid atlasing methodology to build a population of computational models of the coronary arteries to comprehensively and accurately assess anatomy including 3D size, geometry and shape descriptors. A random sample of 122 cardiac CT scans with a calcium score of zero was segmented and analysed using a standardised protocol. The resulting atlas includes, but is not limited to, the distributions of the coronary tree in terms of angles, diameters, centrelines, principal component shape analysis and cross-sectional contours. This novel resource will facilitate the improvement of stent design and provide a reference for hemodynamic simulations, and provides a basis for large normal and pathological databases.

1 Background

Blockage of the coronary arteries causes chest pain, heart attack and sudden death. The prevalence of coronary heart disease (CHD) in the United States is 6.4%, where a myocardial infarction approximately every 44 seconds leads to 1 in 6 deaths being attributable to CHD [6]. The coronary arteries supply oxygen to the heart muscle. Lipid accumulation in the vessel wall (atheroma) narrows the artery, with stenoses particularly likely to develop at sites of altered flow and shear stress such as at the outer flanks of bifurcations [15]. Percutaneous coronary intervention (PCI) is an important treatment for stable atheroma causing chest pain on exertion (angina) and for acute coronary syndromes. This involves the insertion of a guide wire into the artery, balloon expansion, and deployment of a metal or polymer stent to hold the artery open. Each year two million stents

---

* Corresponding author.

are implanted worldwide [6]. Despite anti-proliferative drug coatings on many stents, there are still failures from stent thrombosis by blood clot or in-stent re-narrowing from an excessive neo-intimal proliferative response [1]. Describing the detailed anatomy of the coronary arteries is important for studying the æ-tiology of restenosis: the bifurcation angle has already been found to correlate with major adverse cardiac events at long-term follow-up in patients undergoing PCI [3]. Also, detailed geometry is required for the design of a restricted number of stent sizes and shapes to span a broad range of anatomical diversity, and for computational fluid dynamics simulations (CFD) of blood flow.

There is wide variation in the size and shape of the coronary arteries, and the wire stents provided by manufacturers are not always ideal, especially where the arteries branch. The normal and variant anatomy of the human coronary arteries is well known with a 2009 review [8] describing the embryonic development, nomenclature, and anatomy of the normal and anomalous coronary tree. Several studies have estimated the population variation of bifurcation angle [3, 10, 12] but these have computational and accuracy limitations due to use of 2D angiographic projections, and are often restricted to patients with established disease.

Access to anatomical data beyond labelling of vessels [9, 16], and angular and diameter measurement requires the creation of a large atlas where the detailed tree and shape geometry of the coronaries is stored in a statistical database. Statistical databases of human anatomy have, in the last five years, become a new and important tool for population anatomy.

In this paper, we present the first 3D statistical atlas of human coronary anatomy. Novel contributions include: (i) detailed information not only about the dimensions of the coronary arteries, but also shape and geometry of the coronary arteries and overall coronary tree, (ii) tree statistics applied to coronary centreline structures, and (iii) mesh statistics applied to coronary vessel surfaces.

2   Methods

2.1   Data

A random sample of 122 patients with a calcium score of zero (and therefore very unlikely to have coronary artery disease [7]) were retrospectively selected from a cardiac CT database. The time-point used for the imaging the coronaries was 75% of the cardiac cycle, i.e. during late diastole. Cases with anomalous coronary anatomy (found in less than 5% of the population, e.g. the circumflex originating from the right coronary artery) were excluded from the study [5]. Table 1 shows the demographics of the population.

Patients' consent was sought for the anonymised use of their data according to the local ethical board approval. Images were anonymised and pooled into a DICOM database. OsiriX [11] was used to navigate and manage the database.

2.2   Construction Framework

The open-source plug-in for OsiriX CMIV CTA [14] was used for the generation of the centrelines. The image volume was semi-automatically segmented adhering

Table 1. Sample demographics. Pearson's χ^2 (categorical) and t-test (continuous) p-values are reported between the with- and without-mesh groups.

	With centrelines	With meshes	Without meshes	p-value
N	122	101	21	
Sex	75 F / 47 M	57 F / 44 M	18 F / 3 M	0.0121
Age	55 $\pm$ 8 years	54 $\pm$ 8 years	59 $\pm$ 10 years	0.0224
Height	170 $\pm$ 10 cm	171 $\pm$ 10 cm	164 $\pm$ 8 cm	0.0027
Weight	77 $\pm$ 15 kg	80 $\pm$ 15 kg	65 $\pm$ 10 kg	0.00003
BMI	26.7 $\pm$ 4.4	27.3 $\pm$ 4.4	24.2 $\pm$ 3.3	0.003

to a standardised procedure typically resulting in five centrelines for the left coronary artery (LCA) and two for the right coronary (RCA) for patients with normal anatomy. The segmentation was performed by an experienced analyst and took approximately 20 minutes per case.

Each centreline was manually labelled as one of the following vessels: left anterior descending (LAD), diagonal, septal, left circumflex (LCX), obtuse marginal, intermediate and right coronary artery. The crux was also identified in the RCA when available. If there was more than one vessel fitting the description (such as occurs with multiple diagonal branches), this was also recorded; however only the first sub-branch was used in the analyses. Other available vessels were ignored for this work due to their insufficient sample size ($N < 20$). Bifurcations were automatically calculated from the centrelines.

The centrelines and images were used to generate surface meshes of the vessel wall using specialised software [13] which was possible in 101 cases (83%) – see Fig. 1. In the remainder of cases, a triangular mesh could not be generated due primarily to image limitations such as poor contrast between the arteries and other tissue. The p-values in Table 1 indicate that a mesh was more likely to be generated with higher height, weight and body mass index (BMI). This is currently an area of active research and improved image resolution and better algorithms are increasing success rates [13]. The framework was built in a modular fashion and is independent of the segmentation tool used. In all cases, meshes and centrelines were manually checked for quality.

The atlas therefore comprises centrelines for all patients and meshes for most patients and can be queried for a range of statistical measurements, the methodology of which is divided into centreline and mesh statistics.

2.3   Centreline Statistics

A three-dimensional cubic spline was fitted to the centreline points. To measure the bifurcation angle, a projection plane was defined to be the least-square fit of the set of points containing the bifurcation point and surrounding distal vessel points. This was controlled by a variable arc-length set to between 5-10 mm using a 0.5 mm resolution step. Two angles were analysed within this range: (i) the *incoming* or *tilt angle*, defined as the average angle with which the proximal
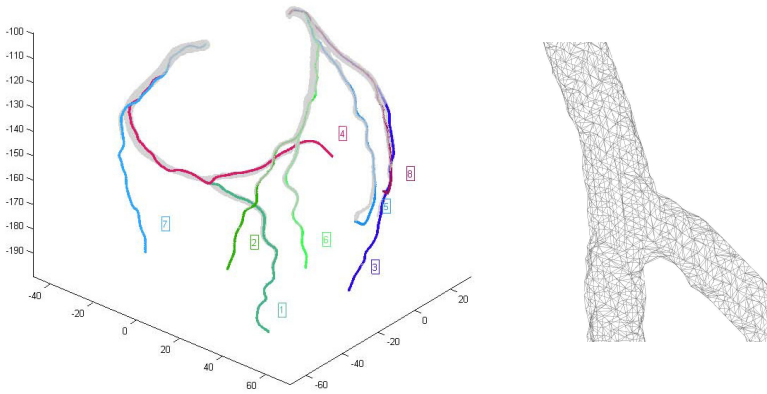
Fig. 1. Left: Single coronary artery tree with numbered centrelines corresponding to vessel description and overlaid semi-transparent mesh in grey. Right: Detail of the wall mesh at a bifurcation.

vessel enters the bifurcation plane, and (ii) the *bifurcation angle*, defined as the average angle between the two distal vessels.

In addition, tree statistics [4] were also applied to define the average left-coronary centreline tree. Tree statistics were recently developed and applied to pulmonary airways and are robust to changes in topology (e.g. when a sub-branch is not present) and are therefore well suited to the anatomy of the coronaries which is highly variable across subjects [5]. They are based on a generalisation of phylogenetic trees where scalar edge lengths have been extended to multi-dimensional edge shape vectors [4]. In our case, these are 8 equidistantly sampled points along each edge of the coronary tree (Fig. 4). In this Euclidean tree space ($t_i \in \mathcal{T}$), a distance between two trees $d(t_1, t_2)$ can be defined as the shortest path between t_1 and t_2 which stays in $\mathcal{T}$ [4]. This distance can be computed recursively and enables the calculation of the Fréchet mean (μ) within our data sample $\mathcal{X} \subset \mathcal{T}$ of $N = 122$ trees, i.e. $\mu = \mathrm{argmin}_{t \in \mathcal{X}} \sum_{i=1}^{N} d^2(t, t_i)$.

2.4   Mesh Statistics

The diameter of the vessel in a plane orthogonal to the centreline was calculated every 0.5 mm along its length, starting from the ostium in the aortic root and ending at the last available point defined by the segmentation algorithm. This resulted in an approximately circular polygon made up of short straight line segments (since the mesh is triangular) which was then used to compute the area, from which average radius can be readily estimated.

The polygons generated from the intersections were also analysed using principal component analysis (PCA). A 15° angular sampling pattern from the centroid of the polygon was used to generate 24 (x, y) pairs on the intersection

plane. Shapes were aligned and scale removed using Procrustes alignment [2]. As an example application, the cross-sectional profile of the left main bifurcation was analysed in three separate regions defined by the distance from the bifurcation point (d): around the bifurcation ($d \leq 5$ mm), and before (proximal) and after (distal) the bifurcation ($5 < d < 15$ mm). These regions are of particular importance for stent design in interventional cardiology.

If the average cross-sectional shape is assumed to be circular as is the case in many CFD papers [15], the atlas can also provide more simplified versions of anatomy which are useful for mechanical experiments such as phase-contrast MRI flow measurements. To facilitate these experiments, a PCA of a simplified model comprising diameters (inlet, bifurcation and outlets) and angles (bifurcation and incoming) was also developed. To overcome the inconsistency of units (mm vs °), the correlation matrix was used.

3   Results

As discussed in section 2.2, the atlas can be queried for a wide range of statistics and user-defined measurements. Due to space limitations, we only show the results for the left main bifurcation, except for the angles.
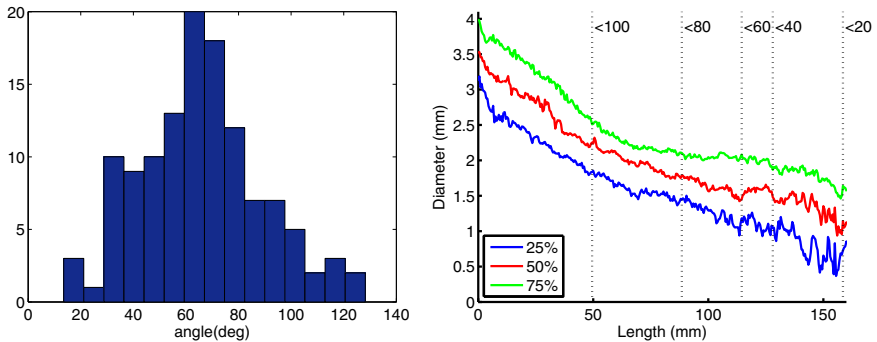

Fig. 2. Left: Histogram of the bifurcation angle between LAD and LCX. Right: Percentile diameters of the LAD plotted at different depths. Vertical lines show the number of cases in the atlas. As the distance increases, and fewer cases are available, the noise increases. Data with fewer than 20 examples are not displayed.

In Fig. 2 left, the distribution of the bifurcation angle between the LAD and LCX is shown. Table 2 shows summary statistics for all angles. In Fig. 2 right, the diameter of the left anterior descending artery is shown throughout its length.

The two principal components of the left main bifurcation 8-variable model are tabulated in Fig. 3.

The average centreline tree was used as a scaffold on which the average diameters were superimposed in Fig. 4, creating a 3D tapered CAD model which combines both centreline and mesh statistics. Also in Fig. 4, we present the results of the cross-sectional analysis in the three areas surrounding the bifurcation as previously discussed.

Table 2. Bifurcation and incoming angles – average ± 1 std. dev. for a range of vessels.

Bifurcation	N	Bifurcation (°)	Incoming (°)
Left main	122	65.8 ± 23.5	22.1 ± 15.3
1st diagonal	92	50.0 ± 15.7	10.7 ± 9.2
Septal	25	50.9 ± 17.2	8.1 ± 6.2
Obtuse marginal	63	51.4 ± 23.6	15.0 ± 12.0
Intermediate with LAD	38	43.2 ± 14.3	15.3 ± 12.4
Intermediate with LCX	38	58.8 ± 18.8	13.9 ± 11.7
RCA acute marginal	68	70.6 ± 25.9	16.0 ± 15.5
RCA crux	83	57.5 ± 22.1	13.9 ± 10.1
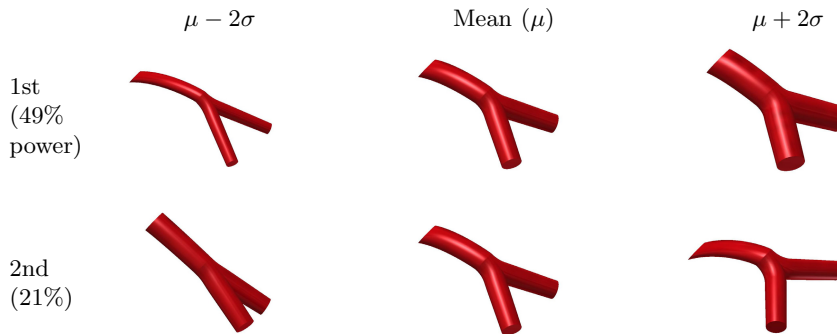
Fig. 3. First and second principal components of the left main bifurcation

4   Discussion

Traditionally, the bifurcation angle has been the only angle investigated; in the best case, this is measured manually using a 3D volume renderer. By using an automated atlasing approach, we have provided a robust measure of the bifurcation and incoming angle. The average left-main bifurcation angle in Table 2 ($66° \pm 24°$) is lower than in previous comparable measurements ([10] reported $80° \pm 27°$ and [12], $74° \pm 25°$), possibly due to sample and methodological differences.

In Fig. 3, the first mode shows how larger diameters tend to have smaller incoming angle whereas the second mode shows the positive correlation of bifurcation and incoming angle. Further work is required to investigate the relationship between these modes and the overall curvature and size of the heart.

The changes in topology across the normal population have been overcome by excluding rare anomalies, and using a flexible framework which allows for missing sub-branches and, in the case of the centrelines, the robust underlying statistics developed by [4]. Point correspondence was implicitly addressed by using the ostia and bifurcations as anchor points, and the arc-length of the centreline.

The combination of one- and two-dimensional statistics can provide tangible computational models, either in a simplified (Fig. 3) or more sophisticated
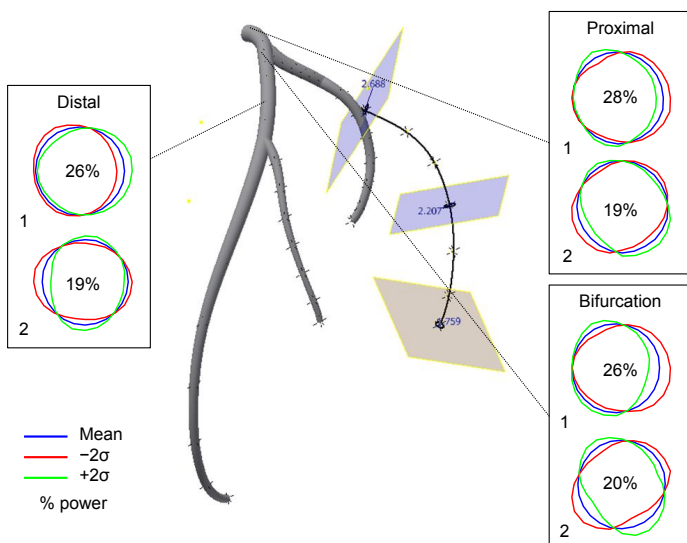
Fig. 4. Average left coronary tree shape with average diameters. The average centreline (shown for the last part of the LCX) is used as a scaffold for the generation of a tapered 3D mesh with real-data average diameters at different points (cross markers). Cross-sectional PCA modes of variation are shown in boxes.

fashion (Fig. 4). These show how the variability of the luminal surface differs in different regions of the tree. With the advent of 3D printers, a variety of applications has emerged for these models, including CFD and stent deployment testing. This is ongoing research in our group.

Other non-uniform sampling patterns based for example on tortuosity could more efficiently represent the centrelines.

We have presented the methodology and preliminary results of the first coronary atlas. We expect to continue to improve this resource with the addition of more cases, both normal and pathological. In the interests of creating public domain databases, we are reviewing our ethical approval in the hope of making the data accessible on-line. In the future, we also expect that the atlas will prove useful for improved stent design.

References

[1] Daemen, J., Wenaweser, P., Tsuchida, K., Abrecht, L., Vaina, S., Morger, C., Kukreja, N., Jüni, P., Sianos, G., Hellige, G., et al.: Early and late coronary stent thrombosis of sirolimus-eluting and paclitaxel-eluting stents in routine clinical practice: data from a large two-institutional cohort study. The Lancet 369(9562), 667–678 (2007)

[2] Dryden, I.L., Mardia, K.V.: Statistical shape analysis, vol. 4. John Wiley & Sons, New York (1998)

[3] Dzavik, V., Kharbanda, R., Ivanov, J., Douglas, J., Bui, S., Mackie, K., Ramsamujh, R., Barolet, A., Schwartz, L., Seidelin, P.H.: Predictors of long-term outcome after crush stenting of coronary bifurcation lesions: importance of the bifurcation angle. Am. Heart J. 152(4), 762–769 (2006)

[4] Feragen, A., Lo, P., de Bruijne, M., Nielsen, M., Lauze, F.: Towards a theory of statistical tree-shape analysis. IEEE Trans. Pattern Anal. Mach. Intell. 35(8), 2008–2021 (2013)

[5] Fiss, D.M.: Normal coronary anatomy and anatomic variations. Appl. Radiol. 36(1), 14–26 (2007)

[6] Go, A.S., Mozaffarian, D., Roger, V.L., Benjamin, E.J., Berry, J.D., Borden, W.B., Bravata, D.M., Dai, S., Ford, E.S., Fox, C.S., et al.: Heart disease and stroke statistics–2013 update: a report from the american heart association. Circulation 127(1), e6 (2013)

[7] Greenland, P., Bonow, R.O.: How low-risk is a coronary calcium score of zero? The importance of conditional probability. Circulation 117(13), 1627–1629 (2008)

[8] Loukas, M., Groat, C., Khangura, R., Owens, D.G., Anderson, R.H.: The normal and abnormal anatomy of the coronary arteries. Clin. Anat. 22(1), 114–128 (2009)

[9] Lu, L., Bi, J., Yu, S., Peng, Z., Krishnan, A., Zhou, X.S.: Hierarchical learning for tubular structure parsing in medical imaging: A study on coronary arteries using 3D CT angiography. In: IEEE 12th Intl. Conf. on Computer Vision, pp. 2021–2028. IEEE (2009)

[10] Pflederer, T., Ludwig, J., Ropers, D., Daniel, W.G., Achenbach, S.: Measurement of coronary artery bifurcation angles by multidetector computed tomography. Invest. Radiol. 41(11), 793–798 (2006)

[11] Rosset, A., Spadola, L., Ratib, O.: Osirix: an open-source software for navigating in multidimensional dicom images. J. Digit. Imaging 17(3), 205–216 (2004)

[12] Rubinshtein, R., Lerman, A., Spoon, D.B., Rihal, C.S.: Anatomic features of the left main coronary artery and factors associated with its bifurcation angle: A 3-dimensional quantitative coronary angiographic study. Catheter. Cardiovasc. Interv. 80(2), 304–309 (2012)

[13] Wang, C., Frimmel, H., Smedby, Ö.: Level-set based vessel segmentation accelerated with periodic monotonic speed function. In: SPIE Medical Imaging, p. 79621M. International Society for Optics and Photonics (2011)

[14] Wang, C., Smedby, Ö.: Coronary artery segmentation and skeletonization based on competing fuzzy connectedness tree. In: Ayache, N., Ourselin, S., Maeder, A. (eds.) MICCAI 2007, Part I. LNCS, vol. 4791, pp. 311–318. Springer, Heidelberg (2007)

[15] Williams, A.R., Koo, B.K., Gundert, T.J., Fitzgerald, P.J., LaDisa, J.F.: Local hemodynamic changes caused by main branch stent implantation and subsequent virtual side branch balloon angioplasty in a representative coronary bifurcation. J. Appl. Physiol. 109(2), 532–540 (2010)

[16] Yang, G., Broersen, A., Petr, R., Kitslaar, P., de Graaf, M.A., Bax, J.J., Reiber, J., Dijkstra, J.: Automatic coronary artery tree labeling in coronary computed tomographic angiography datasets. In: Computing in Cardiology, pp. 109–112. IEEE (2011)